An Optical Fiber Monolith Reactor for Photocatalytic Wastewater Treatment

Hongfei Lin and Kalliat T. Valsaraj
Gordon A. and Mary Cain Dept. of Chemical Engineering, Louisiana State University, Baton Rouge, LA 70803

DOI 10.1002/aic.10823
Published online March 24, 2006 in Wiley InterScience (www.interscience.wiley.com).

A two-dimensional (2-D) mathematical model to describe the photocatalytic degradation of aqueous-phase organic compounds in a multichannel optical fiber monolith reactor (OFMR) was developed and validated by experimental results. The model incorporated an empirical radiation field submodel, an annular flow dynamics submodel, and a Langmuir–Hinshelwood kinetics submodel. Parameters for the radiation field submodel were derived experimentally. The rate constant in the model accounted for both surface adsorption rate and intrinsic reaction rate. The model presented may be used for the design and optimization of the OFMR. Satisfactory agreement between the model predictions and experimental results over a range of experimental conditions was observed. The effects of the reactor geometry including the fiber diameter, the ratio of the fiber diameter, and the channel diameter and the reactor length were investigated. Higher efficiency of degradation was observed for the reactor with the larger fiber and smaller ratio of the fiber diameter to the channel diameter at the expense of a lower liquid throughput. The reactor efficiency was higher in the upflow mode than in the downflow mode for the water stream. © 2006 American Institute of Chemical Engineers *AIChE J,* 52: 2271–2280, 2006

Keywords: monolith reactor, optical fiber, photocatalysis, water treatment, reactor model, phenanthrene, dichlorobenzene

Introduction

Heterogeneous photocatalysis using low-energy UV-irradiated TiO_2 has been shown to be an effective means of removing organic pollutants from water.[1-6] There are still numerous barriers for the successful commercialization of heterogeneous photocatalysis as an alternative method for wastewater treatment.[5-7] The rigorous modeling of photocatalytic reactors requires a complex analysis of the submodels of the radiation field, the fluid dynamics, and the reaction kinetics, which are crosslinked to the material and energy balances in the photoreactor,[8,9] and results in integral–differential equations that require demanding numerical solutions. Simpler models obtained by decoupling the substrate concentration field and the radiation field are easier to use for scale-up and design purposes.[10] Thus, the development of simple mathematical reactor models is especially important to assist the design, scale-up, and optimization of the photocatalytic reactors on an industrial scale.[8]

The most widely deployed photoreactor design is the annular flow configuration with immobilized photocatalyst, and modeling of this type of reactor has been done extensively for both water and air purification.[10-12] However, such reactors are limited to the laboratory scale because of low-light use efficiencies and mass transport limitations within the fluid phase.[7] Recently we proposed a distributive optical fiber monolith reactor (OFMR),[13] which provides a higher surface area for catalyst coating per unit reactor volume compared to that of annular reactors. This was based on previous designs by other investigators of a fiber-optic cable reactor[16,20] and ceramic monolith reactor.[21] The OFMR is composed of a ceramic monolith with large number of parallel channels into each of which a fiber-optic cable is inserted. The conditions in each channel are presumed to be identical when assuming uniform

Correspondence concerning this article should be addressed to K. T. Valsaraj at Valsaraj@lsu.edu.

distribution of variables such as flow flux and radiance flux at the monolith cell inlet and outlet. A single channel with a fiber inserted is considered as an individual mini-annular reactor because the optical fiber is used for the UV light conduction. In a conventional immobilized annular reactor, either the reactor wall or the lamp casing is coated with the photocatalyst. Thus, only one surface of the annuli is used as the reaction site. In an OFMR, both the channel wall and the outside of the fiber in each channel are coated with TiO_2 and both function as reaction sites. The presence of such a large number of channels within the OFMR not only provides a larger surface area for reaction, but also improves the liquid throughput through the reactor.

We developed a simple model to describe the degradation of a compound in an OFMR by incorporating an empirical submodel of the radiation field, which is decoupled from the concentration field of the substrate. In this paper, experiments on bench-scale OFMR was also conducted under a variety of conditions including intensity of input light, flow velocity, direction, and reactor geometry. The experimental results were compared with the model-predicted results to validate the feasibility of the model. Phenanthrene (PHE) and 1,2-dichlorobenzene (DCB) were selected as the target organic contaminants for the photocatalytic experiments to be consistent with our previous works.[12-14] The primary aim of this work is to provide—by a combination of modeling and experiments—a design of our current reactor.

Experimental

Materials

Phenanthrene of 98% purity was obtained from Aldrich Chemicals (Milwaukee, WI). 1,2-Dichlorobenzene of 98% purity was obtained from EM Sciences (Gibbstown, NJ). Powered titania (P25) from Degussa Corporation (Akron, OH) was used as the photocatalyst. The TiO_2 crystallites had a mean surface area of 60–70 $m^2\ g^{-1}$, a mean particle diameter of 20 nm, and the point of zero charge at a pH of 6.8.

Characterization of TiO_2 coating

Two kinds of multimode quartz optic fibers (3M Power-Core FT-1.0-UMT and FT-400-UMT) with diameters of 0.001 and 0.0004 m, respectively, were purchased from Thorlab (Newton, NJ) and used as the UV light conductor. The optic fiber wire was cut into multiple pieces, each with a length of 0.9 m. A section of the single fiber was then stripped to the desired length and the quartz core exposed. A dip-coating method was used to immobilize TiO_2 particles on the outer wall of the quartz optic fiber and the inner walls of the monolith substrate. TiO_2 suspensions of 0.125, 0.25, 0.5, 1, 2, and 5 wt % were used to coat the optic fibers, whereas a 20 wt % suspension was used to coat the monolith channels. The details of coating method were described in our previous report.[13]

Multichannel optical fiber monolith reactor assembly

A schematic of the experimental assembly including the multichannel optical fiber monolith reactor is given in Figure 1. The reactor details were given in our previous paper describing the proof-of-concept.[13] All 61 channels of the monolith were used for the fiber with 0.0004 m diameter. However, only 19 channels of the monolith were used for the 0.001 m diameter fiber. The rest of the channels were blocked permanently by using high-temperature epoxy resist. The cross-sectional area of the fiber bundles in both cases was the same, 7.85×10^{-4} m^2. The length of the monolith block was 0.30 m with a channel diameter of 0.003 m. However, as described earlier,[13] only a portion of the length of the fiber was effective in light transmission and thus the overall effective length of the reactor was much smaller than 0.30 m.

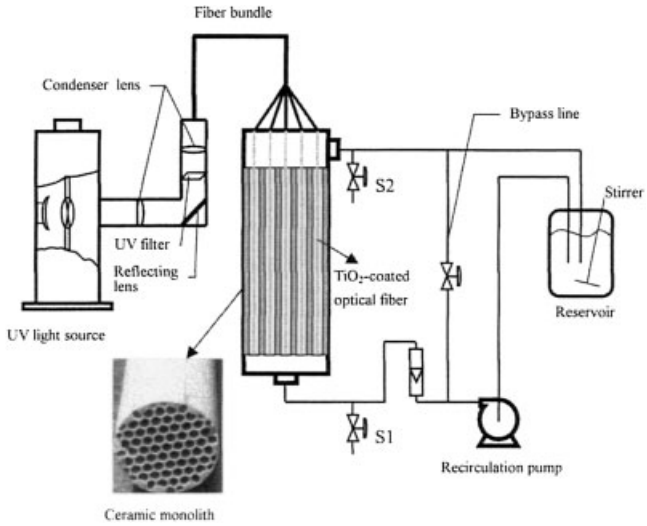

Figure 1. Optical fiber monolith reactor (OFMR) and experimental setup.

Note that the reactor was operated in the continuous recycle mode. Samples were taken at S1 and S2 to determine the overall removal efficiency.

Two types of 500-W Xe short-arc lamp (Osram XBO 500W/R and Osram XBO 500W/H), obtained from Spectral Energy Corporation (Washingtonville, NY), were used as the UV radiation source. The former type of lamp provided higher light intensity and was used for the OFMR with small fibers to ensure that both TiO_2 coatings (outer fiber surface and the monolith wall) were well illuminated. The overall operation was in the continuous recycle mode with multiple passes through the reactor. The inlet and outlet samples were collected at valve ports S1 and S2, respectively.

Methodology and chemical analysis

The DCB or PHE solution was recirculated through the reactor in the dark (that is, without UV light) for 2 h to ensure that adsorption equilibrium was reached. After 2 h the UV lamp was turned on. The overall reaction loss of DCB or PHE was obtained by sampling the influent and effluent at 20-min intervals. The DCB in the aqueous sample was extracted into hexane. The hexane extract was analyzed using a gas chromatograph (Model HP 6890, Hewlett–Packard, Palo Alto, CA) coupled with a mass spectrometer (HP 5973). The PHE in the aqueous sample was analyzed using a high-performance liquid chromatograph (HP 1100, Hewlett–Packard). A detailed description can be found in our previous papers.[12,14] The incident UV light intensity was measured by a UV radiometer (UVP UVX radiometer) coupled with a 365-nm sensor (UVX-36 long-wave sensor).

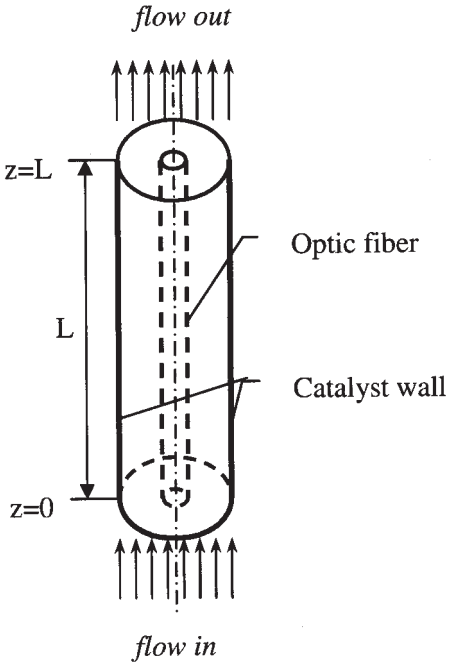

Figure 2. Single monolith cell with a TiO_2-coated optical fiber inserted.

The channel wall is also coated with TiO_2. At reactor inlet, $z = 0$; at reactor outlet, $z = L$. L is the coating length or the effective reactor length.

Results and Discussion

Development of the mathematical model

Figure 2 shows the schematic of a single monolith cell with TiO_2-coated optical fiber inserted. Under the hypothesis that all monolith channels are identical, the simulation of the entire multichanneled monolith reduces to the analysis of a single channel. We set up a single-channel monolith model that incorporated a representation of the developing flow field and simultaneous liquid-phase diffusion and heterogeneous reaction. This model also included the influence of the UV light radiance flux, which was based on the light transmission submodel in our previous work.[15] Apart from the assumption that all channels are identical, we make the following assumptions to simplify the problem: annular symmetry of the monolith channel irradiated by a TiO_2-coated optical fiber placed in the center of the channel; dilute contaminants in water; and unsaturated active sites on the surface of titania films. We assumed that the primary heterogeneous reaction takes place at the surface of TiO_2 films on the optical fiber and the channel wall and homogeneous photolysis reactions in the bulk water phase were negligible. We also assumed that the reaction was not limited by O_2 sorption or by competitive inhibition from reaction intermediates or other solution species. This assumption was made to simplify the model, even though reaction intermediates might significantly affect the reaction rate of the parent compound.

Fluid-dynamic model

Assuming steady-state, unidirectional, incompressible, continuous flow under a fully developed laminar regime in the annular channel, the velocity profile in a radial section of the annulus can be expressed as follows[17]:

$$v_z(r) = \frac{2u}{\left[(1+\eta^2) - \dfrac{(\eta^2-1)}{\ln \eta}\right]} \times \left[1 - \left(\frac{r}{R_w}\right)^2 + \left(\frac{\eta^2-1}{\ln \eta}\right)\ln\left(\frac{r}{R_w}\right)\right] \quad (1)$$

where r is an arbitrary radial position in the annulus; R_w is the radius of monolith channel or the external radius of annulus; and u, the superficial flow velocity through the annulus, is expressed as

$$u = \frac{Q}{\pi R_w^2(1-\eta^2)} \quad (2)$$

where Q is the volumetric flow rate through the annulus and η is the ratio of the fiber radius to the monolith channel radius or the ratio of internal radius to external radius of annulus, expressed as

$$\eta = R_f/R_w \quad (3)$$

where R_f is the radius of the fiber or the internal radius of annulus. Equation 1 is valid for laminar flow only, which occurs when

$$N_{\mathrm{Re}} = \frac{2R_w(1-\eta)u\rho}{\mu} \leq 2000 \quad (4)$$

For a dilute aqueous solution, we approximated the density and viscosity of the solution to those of pure water at room temperature. In this study, the Reynold's number (Re) was between 1 and 11, and thus Eq. 4 was satisfied.

Reaction kinetics model

The kinetic rate equation used in the present model was derived based on the following: (1) the rates of photocatalytic destruction of organic contaminants can be fitted by a Langmuir–Hinshelwood kinetic rate equation; (2) the kinetic rate constant follows a power-law expression of the total radiation absorbed in the TiO_2 coating layers on the outer surface of the optical fiber and the inner surface of the monolithic channel[22]:

$$-r_{As} = kI^n \frac{KC}{1+KC} \quad (5)$$

where K refers to the adsorption equilibrium constant; n is the power-law coefficient, which varies between 0.5 and 1 depending on the light intensity (the suggested threshold value is 25 mW cm^{-2} by Herrmann[5] or 6 mW cm^{-2} by Peill and Hoffmann[16]); and C is the reactant concentration. The light intensity I, at the illuminated TiO_2 surface inside a monolithic channel, was low and n was safely assumed to be 1 without introducing large error. k is an observed rate constant that takes into

account the major factors that affect the overall destruction rate: the intrinsic surface reaction rate (k_s), quantum yield of photodegradation of the contaminant (Φ), TiO_2 film absorptivity for UV light (ε), and the concentration of total active reaction sites on the TiO_2 film (C_a):

$$k = k_s \phi \varepsilon C_a \tag{6}$$

The present kinetic rate equation does not include the effect of reaction intermediates because most of the applications of photocatalytic detoxification involve lightly contaminated water in which the effect of the intermediates can often be neglected. For very dilute wastewater streams, $KC \ll 1$ and Eq. 5 is simplified to yield

$$-r_{As} = k_T I C \tag{7}$$

where k_T is the total rate constant that takes into account all other major factors that affect the overall destruction except the concentration of the substrate:

$$k_T = k_s K \phi \varepsilon C_a \tag{8}$$

Material balance

With reference to Figure 1, the equation of convective diffusion in the annulus is

$$v_z(r) \frac{\partial C_A}{\partial z} = \frac{D}{r} \frac{\partial}{\partial r} \left(r \frac{\partial C_A}{\partial r} \right) \tag{9}$$

where $v_z(r)$, C_A, and D denote the axial velocity, concentration of species A, and diffusion coefficient, respectively. In this unit, the photocatalyst was deposited onto the inner surface of the channel. The stripped optic fiber was placed in the center of the channel and was used to conduct the UV light. The boundary conditions on the fiber titania coating and monolith coating are

$$D \frac{\partial C_A}{\partial r} = r_{As} \qquad r = R_f \tag{10}$$

$$D \frac{\partial C_A}{\partial r} = r_{As} \qquad r = R_w \tag{11}$$

At the reactor inlet,

$$C_A = C_{in} \qquad z = 0 \tag{12}$$

If the reactor is in the diffusion control region, the reactant A is quickly consumed on the titania surface and the boundary conditions at $r = R_f$ and $r = R_w$ become

$$C_A = 0 \qquad r = R_f \tag{13}$$

$$C_A = 0 \qquad r = R_w \tag{14}$$

This is normally the case with certain photocatalytic reaction with high quantum yields and rapid kinetics. Therefore, the extent of conversion depends on the rate of transport of target species to the titania surface from the bulk solution.

The equation of convective diffusion written in terms of species concentration and reactor length can be transformed into one in terms of conversion in a single pass, $x = 1 - (C_A^{out}/C_A^{in})$, and time t by allowing $u = \partial z/\partial t$, where u is the superficial velocity independent of z. This implies the cross-sectional geometry of the reactor is constant and the diffusion in the main direction of the convective flow can be neglected. Also using dimensionless form of $\bar{r} = r/R_w$, then Eq. 9 becomes

$$u_{dl} \frac{\partial x}{\partial t} = \frac{D}{R_w^2} \frac{\partial}{\partial \bar{r}} \left(\bar{r} \frac{\partial x}{\partial \bar{r}} \right) \tag{15}$$

where u_{dl} is a function of $\bar{r}$, given by

$$u_{dl} = \frac{v(\bar{r})}{u} = \frac{2}{\left[(1 + \eta^2) - \dfrac{(\eta^2 - 1)}{\ln \eta} \right]} \times \left[1 - \bar{r}^2 + \left(\frac{\eta^2 - 1}{\ln \eta} \right) \ln \bar{r} \right] \tag{16}$$

The boundary conditions for reaction control are

$$D \frac{\partial x}{\partial \bar{r}} = k_T I_f (1 - x) \qquad \bar{r} = \eta \tag{17}$$

$$D \frac{\partial x}{\partial \bar{r}} = k_T I_w (1 - x) \qquad \bar{r} = 1 \tag{18}$$

where I_f is the light intensity on the fiber coating, the equation for which was obtained experimentally elsewhere[15]:

$$I_f = \frac{1}{4} d_f \{ \alpha f_\theta \exp[-(\alpha z + \varepsilon \delta)] I_{input} + \beta \exp[-\beta(L - z)] I_{output} \} \tag{19}$$

where δ is the thickness of the TiO_2 film on the fiber. α, β, ε, and f_θ are the fitting parameters. I_{input} is the input light intensity at the top end tip of the fiber ($z = 0$) and I_{output} is the light intensity at the bottom end tip of the fiber ($z = L$):

$$I_{output} = [(1 - f_\theta) + f_\theta \exp(-\alpha L)] I_{input} \tag{20}$$

I_w is the light intensity on the monolith channel wall coating:

$$I_w = \eta I_f \tag{21}$$

Here, per fiber I_{input} equals the measured total incident light intensity, I_0, divided by the total number of fibers within a fiber bundle, N_f. The total incident light was collected by the polished fiber bundle tip end. Given the same cross-sectional area of the fiber bundle, for large fibers of 0.001 m diameter, $N_f =$

Table 1. Optical Fiber Monolith Reactor Model Parameters

Type	Model Parameters	Values	Unit
Geometry	d_f	0.001; 0.0004	m
	R_w	0.0015	m
	R_f	0.0005; 0.0002	m
	L	0.05; 0.10; 0.20	m
	η	0.333*; 0.133**	dimensionless
	δ	241; 390; 603; 1036; 1660; 4114	nm
Fluid dynamics	u	3.86×10^{-4}–11.57×10^{-4} * 11.75×10^{-4}–56.5×10^{-4} **	m s^{-1}
	N_{Re}	1.003–3.008*; 2.35–11.3**	dimensionless
Mass transfer	D	PHE: 0.437×10^{-9} DCB: 0.89×10^{-9}	m^2 s^{-1}
Radiation field	α	38.6*; 77.7**	m^{-1}
	f_θ	0.762*; 0.967**	dimensionless
	β	195	m^{-1}
	ε	0.00102	nm^{-1}
Kinetics	k_T	PHE: $(1.57 \pm 0.01) \times 10^{-4}$ DCB: $(1.08 \pm 0.09) \times 10^{-4}$ †	m^2 s^{-1} mW^{-1}

*Using small fiber with diameter of 0.0004 m.
**Using large fiber with diameter of 0.001 m.
†Estimated using experiments at different light intensities described by Lin.[15]

19; and for small fibers of 0.0004 m diameter, $N_f = 61$. The boundary conditions for mass transfer control are

$$x = 1 \qquad \bar{r} = \eta \tag{22}$$

$$x = 1 \qquad \bar{r} = 1 \tag{23}$$

The initial condition is

$$x = 1 \qquad t = 0 \tag{24}$$

The mean cup conversion is given by

$$x_m = \frac{2}{1 - \eta^2} \int_\eta^1 x u_{dl} \bar{r} d\bar{r} \tag{25}$$

Optical fiber monolith reactor with recycle

In a continuous reactor system in which all the flow emerging from the outlet of the photoreactor ware circulated to the inlet passing through an ideal well-mixed reservoir, which was assumed to be a continuous flow stirred tank reactor (CSTR), the number of passes N_p of the aqueous solution through the reactor in a given time t was

$$N_p = \frac{t}{\tau_{reactor}} = t \frac{Q}{V_{reactor}} \tag{26}$$

where V_r and τ are the volume and the space time of the reactor, respectively. The rigorous analysis of the present recirculation system requires solving the system of the time-dependent differential equations for the reactor and the reservoir. However, by assuming that the conversions per pass are small (valid when $V_{reactor} \ll V_{reservoir}$), which are conditions usually verified in most experimental recirculation photocatalytic reactor systems including ours, the differential form was simplified to a discrete form. With the above assumption, it was sufficient to process the equivalent of one reactor volume of liquid in the time interval of $\Delta t = \tau_{reactor}$. Equation 24 can be used to calculate the conversion of a single pass of one reactor volume of processed liquid. The new inlet concentration to the reactor after each pass was calculated by a material balance in the reservoir, which yielded

$$C_i^{in}(t) = (1 - \lambda) C_{i-1}^{in}(t - \tau_{reactor}) + \lambda C_i^{out}(t) \tag{27}$$

where λ is the ratio of the reactor volume to the reservoir volume:

$$\lambda = \frac{V_{reactor}}{V_{reservoir}} \tag{28}$$

The procedure is iterated for N_p number of passes to yield the final concentration, $C_{N_p}^{out}(t)$, after a time $t = N_p \tau_{reactor}$. The final conversion was therefore

$$x_T(t) = 1 - \frac{C_{N_p}^{out}(t)}{C_0} \tag{29}$$

where C_0 is the initial concentration of the substrate in the reservoir. In our previous finding,[13] the conversion of each single pass was constant within a narrow range of inlet concentrations, that is, the fraction removal was independent of the inlet concentration; thus iterating Eq. 27 yielded the inlet concentration, $C_{N_p}^{out}(t)$, and the outlet concentration, $C_{N_p}^{out}(t)$, at $t = N_p \tau_{reactor}$:

$$C_{N_p}^{in}(t) = (1 - \lambda x)^{N_p} C_0 \tag{30}$$

$$C_{N_p}^{out}(t) = (1 - x)(1 - \lambda x)^{(N_p - 1)} C_0 \tag{31}$$

Evaluation of model parameters

The estimated parameters and the constants in the reactor model are summarized in Table 1. The predicted reactor conversions can then be computed for given values of the inlet flow velocity, inlet substrate concentration, and input light intensity. The geometrical parameters were measured and calculated according to the dimensions of the reactor. The parameters that describe the fluid dynamics of the liquid phase (viscosity and density) were assumed to be those of pure water at room temperature. The experimental parameters for the description of the radiation field were given elsewhere.[15] The diffusion coefficients of the substrates (PHE and DCB) in water were obtained from the literature.[18] The only other parameter in the model, the specific rate constant k_T, was estimated by first fitting the model to the experimental results under different light intensity conditions for each compound.[15] The values of k_T for each compound were observed to have little variability (Table 1). As shown in Table 1, the diffusion coefficient of DCB was larger than that of PHE but the rate constant for DCB was smaller than that of PHE. Once these parameters have been estimated, the predicted single-pass reactor conversions were computed for given values of the inlet flow velocity, the inlet substrate concentration, and the input light intensity. The overall multiple-pass conversions of the reactor with recycle were further obtained.

Model simulations and comparison with experimental data

The model equations including the submodel equations of radiation field described by Lin[15] constitute a system of nonlinear differential equations with complex nonlinear boundary conditions. FEMLAB® was used to solve for the single-pass conversion. With r varying from R_f to R_w, Eq. 25 was integrated numerically to obtain the average conversion of the substrate at the reactor outlet. Equations 10–14 were numerically solved to calculate the radial profile of the dimensionless substrate concentration at the reactor outlet.

Using the above parameters the model simulations were compared to the experimental results under various experimental conditions. Figures 3a and 3b compare the model-predicted results to experimental multiple-pass data for PHE and DCB photooxidation. The experiments were operated in a continuous flow recycle mode, the details of which were previously described.[13] It should be noted that the primary aim of the work described here was the overall design and modeling—but not the optimization—of the reactor for maximum efficiency. Figures 4a and 4b depict the model predictions for PHE and DCB degradation, compared to experimental single-pass data at various flow rates. Figures 5 a and 5b compare the model and experimental results under different intensities of the incident light.

Two limiting cases were considered: a reaction-limited regime and a mass transfer (diffusion)–limited regime. Overall, the model based on the assumption that surface reactions are the dominant rate-controlling step was found to fit the experimental results satisfactorily within the ranges of the parameters investigated. The only exception was at low flow velocity (or low Reynold's number), in which case the model overestimated the conversion as shown in Figures 4a and 4b. This can be explained by the mass transfer rate limitation that adversely

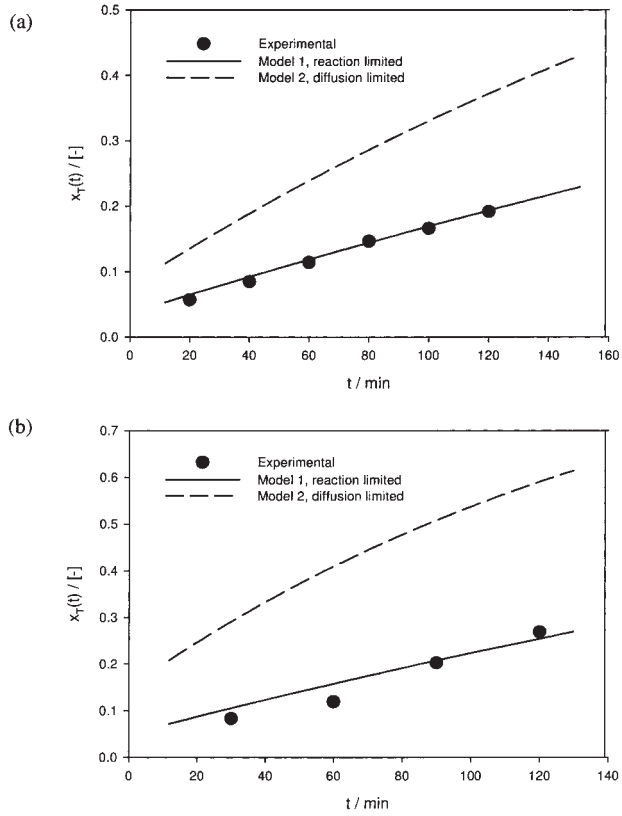

Figure 3. Overall conversion for photocatalytic oxidation of (a) PHE and (b) DCB in continuous recycling multipass runs in an OFMR.

Geometry: d_f = 0.001 m; η = 1/3; L = 0.10 m. Experimental conditions: $C_{0,\mathrm{PHE}}$ = 639 ppb; $C_{0,\mathrm{DCB}}$ = 180 ppb; u = 0.34 m min^{-1}, $I_0 = 3.14 \times 10^4$ mW m^{-2}.

affects the removal efficiency at low Reynold's number. On the other hand, the model based on the assumption that diffusion of reactants to the catalyst surface is the rate-limiting step, which implies extremely fast reaction rates, vastly overestimated the conversion compared with the experimental data obtained at all conditions. This suggested that the surface reaction rates were not fast enough to create a completely mass transport limited regime.

Effects of geometric parameters

The ratio of fiber diameter to the monolith channel diameter η, the fiber diameter d_f, and the fiber coating length L are important geometric parameters in the design and optimization of the OFMR. Compared to the conventional annular reactors, the light transmission and distribution inside a channel of the OFMR are more sensitive to the changes in these geometric parameters. Thus, the overall removal efficiency of the substrate is further significantly affected by the geometric parameters in the OFMR.

The effects of fiber diameter in OFMR design are much more complex and should be considered comprehensively. First, fiber diameter determines the ratio (η) for a given monolith channel radius and thus affects the extent of mass transfer. Second, increasing fiber diameter provides a larger TiO_2-coating surface area by increasing the outer surface area of the fiber

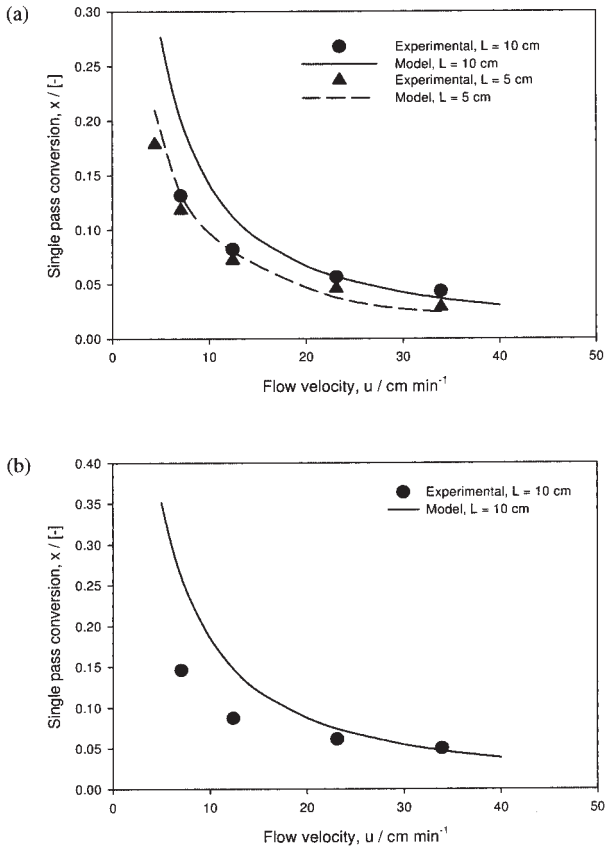

Figure 4. Single-pass conversion for photocatalytic oxidation of (a) PHE and (b) DCB at different flow velocities in an OFMR.

Geometry: $d_f = 0.001$ m; $\eta = 1/3$. Experimental conditions: $C_{0,\mathrm{PHE}} = 562$–711 ppb; $C_{0,\mathrm{DCB}} = 2113$–$2705$ ppb; $I_0 = 3.14 \times 10^4$ mW m^{-2}.

and extending the light propagation length. Third, fiber diameter considerably affects the fitting parameters in the radiation field, which is extensively discussed in a recent thesis.[15] Finally, fiber diameter determines the fiber number density in a fiber bundle with a given cross-sectional area and thus the monolith channel number. It further affects the quantum efficiency with the given incidental light intensity[19] and the throughput of the reactor or the flow velocity. Figure 7 shows the experimental overall conversion of PHE in the two reactors with fiber diameters of 0.001 and 0.0004 m, respectively. The TiO_2-coating length or the effective reactor length was 0.05 m. The fiber coating thickness was 390 nm. The total incident light intensity was kept at 5.966×10^4 mW m^{-2}. The number of fibers or channels was 19 for the large fiber and 61 for the small fiber. The flow rate was 14.8×10^{-6} m^{-3} min^{-1} and the flow velocities were 0.124 and 0.035 m min^{-1}, respectively. The initial concentration of PHE was about 450 ppb. At a given input light flux and flow velocity, the overall conversion of PHE in the OFMR with the large fiber was higher than that with the small fiber. Further investigation of the model-predicted[15] radial and axial profiles of the dimensionless concentration noted that when the small fiber of 0.0004 m diameter was used, the reaction on the surface of the monolith channel wall coating was very low as the result of a lack of photons (Figure 6). Therefore, the illuminated TiO_2 surface area of the OFMR using small fibers was less than that using large fibers. However, for a given effective reactor length the total TiO_2 coating surface area of the OFMR with small fibers was higher because of the larger number of channels. Sufficient light illumination on the monolith channel wall coating must be obtained when using a small fiber diameter in the OFMR design. When an extremely high light intensity was applied for small fibers, it minimized the negative light intensity effects on quantum yield while maintaining rapid overall degradation rates. In this case, the same input light flux can be divided by a larger number of fibers and distributed into more monolith channels. However, even though the incident light intensity was high, we cannot conclude that the performance of an OFMR using small fibers would be superior to that of an OFMR using large fibers because the above comparison is based on the same active catalyst coating length.

It was observed that as the fiber diameter increased, the light propagation along the fiber was extended because photons underwent fewer reflections at the quartz–titania interface for a fixed incident angle. The coating length or the effective reactor length was thus extended with a large-diameter fiber and the activated photocatalytic surface area was enhanced. Measurements of the light intensity profile of a single fiber showed[15] that the effective light propagation length of the 0.0004 m diameter TiO_2-coated fiber was only 0.05 m, whereas that for the TiO_2-coated fiber of 0.001 m diameter was 0.20 m. There-

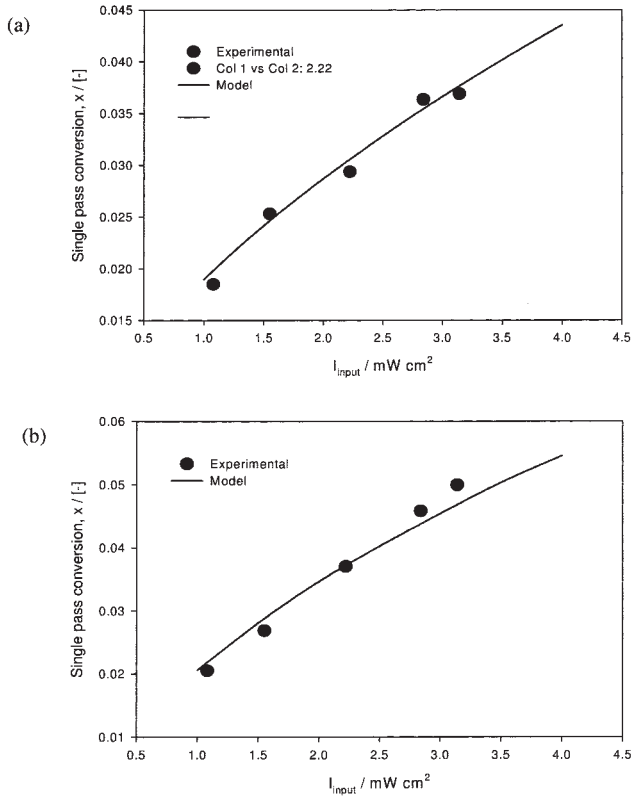

Figure 5. Single-pass conversion for photocatalytic oxidation of (a) PHE and (b) DCB at different input light intensities in an OFMR.

Geometry: $d_f = 0.001$ m; $\eta = 1/3$. Experimental conditions: $C_{0,\mathrm{PHE}} = 639$ ppb; $C_{0,\mathrm{DCB}} = 4796$ ppb; $u = 0.34$ m min^{-1}.

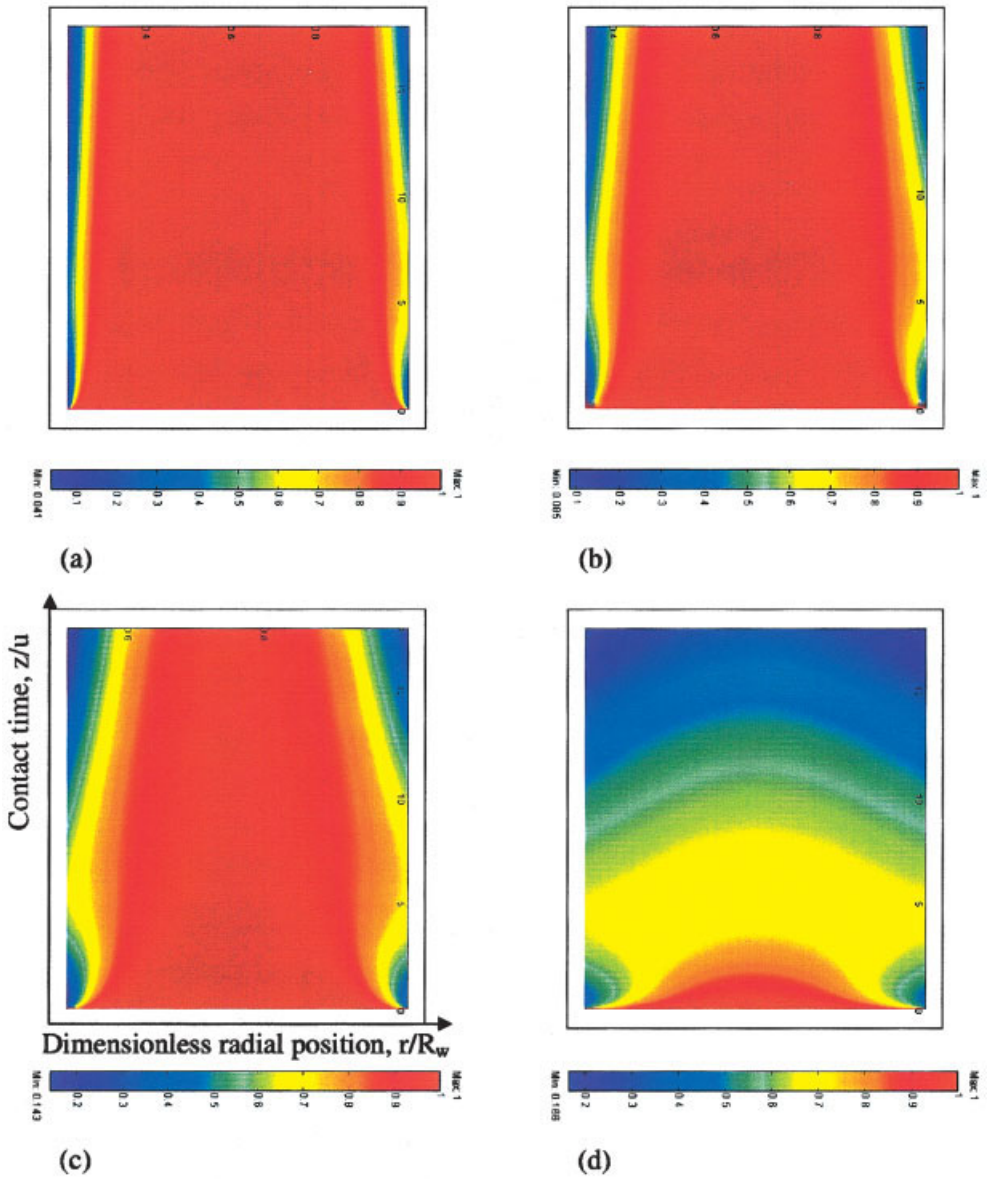

Figure 6. Model simulation for photocatalytic oxidation of PHE in a single channel of OFMR.

Radial profiles of the dimensionless concentration along the axial direction from the reactor inlet. Geometry: $d_f = 0.001$ m; $\eta =$ (a) 1/5; (b) 1/3; (c) 1/2; (d) 5/6; $L = 0.1$ m. Experimental conditions: $C_0 = 639$ ppb; $u = 0.34$ m min^{-1}. Note: the scale of dimensionless radius is not the same.

fore, the illuminated TiO_2 coating surface area was fourfold higher when using the fiber of 0.001 m diameter than the 0.0004 m diameter in a single monolith channel.

Unlike the conventional photocatalytic reactors, the reactor length of an OFMR is not an independent design parameter. Instead, the reactor length is determined by the effective light propagation length along the TiO_2-coated fiber in an OFMR. Any reactor length longer than the effective light propagation length will be poorly used. With the assistance of the model, Figure 8 predicts the single-pass conversion for PHE degradation. As shown in Figure 8, when the reactor length was shorter than the effective light propagation length, the single-pass conversion increased linearly with the reactor length. However, once the reactor length exceeded the effective light propagation length, only marginal enhancement of the conversion was obtained.

Effects of feed flow direction

Figure 9 shows the photodegradation efficiency of phenanthrene under conditions of different flow directions (upflow and downflow) for water in the reactor. It is clear that the efficiency in the downflow mode is lower at small influent feed rates, but becomes similar to that of the upflow mode at high flow rates. It is well known that at flow rates such as those used here in the downflow mode, the flow pattern inside the annulus can be characterized as film flow.[23] We can envisage two films: one over the TiO_2 on the fiber and one over the TiO_2-coated

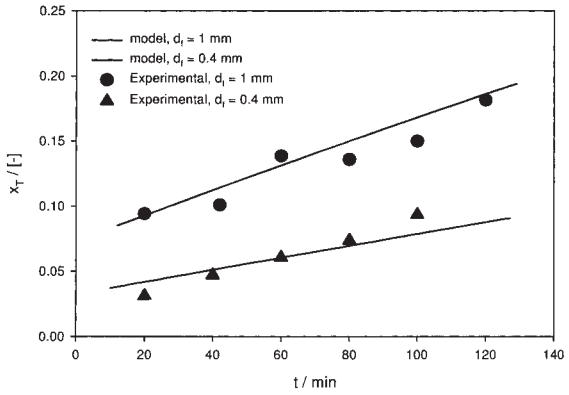

Figure 7. Effect of fiber diameter on the overall conversion of PHE in recycling flow mode in multichannel OFMR.

$L = 0.05$ m; $\varepsilon = 390$ nm; $C_0 = 450$ ppm; $Q = 1.48 \times 10^{-6}$ m^3 min^{-1}; $I_0 = 59 \times 10^4$ mW m^{-2}.

ceramic wall. The light transmission occurs from the fiber to the wall over two air/water interfaces and the incident light on the ceramic wall will be substantially reduced. Thus although mass transfer of phenanthrene to the catalyst may be better, light utilization will be poor in the downflow mode. In the upflow mode, because the channels are filled with water, the light transmits from the fiber to the wall across the water film. Although mass transfer is still a potential problem, the catalyst activation by UV light may be more favorable. At higher flow rates, the flow pattern in both modes is characterized as annular flow[23] and light transmission patterns may coincide. Overall, the upflow mode provided better efficiencies for phenanthrene degradation.

Conclusions

A two-dimensional heterogeneous convective–diffusion–reaction model was developed to simulate the performance of a multichannel optical fiber monolith reactor. With the assumption of identical channels, the multichannel reactor model was reduced to a single-channel reactor model without losing the essential elements of the reactor. The reactor model incorporated an empirical radiation field submodel, an annular flow dynamics submodel, and a Langmuir–Hinshelwood kinetics submodel. The total rate constant considered both surface adsorption rate and intrinsic reaction rate. This simple model may be suitable for use in design, scale-up, and optimization of an OFMR system because the model parameters can be easily estimated or measured. Reasonable agreement was found between the model-predicted and experimental photodegradation conversion data within the limits of experimental error.

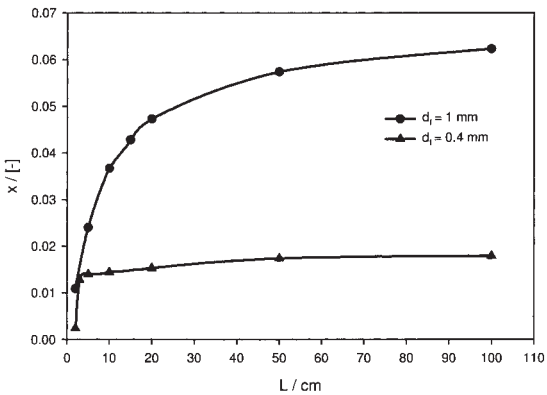

Figure 8. Model simulation for photocatalytic oxidation of PHE in a single-pass run in the OFMR.

Effect of the reactor length on the single-pass converion. Geometry: $R_\Psi = 0.0015$ m. Experimental conditions: $u = 0.34$ m min^{-1}, $I_0 = 59 \times 10^4$ mW m^{-2}.

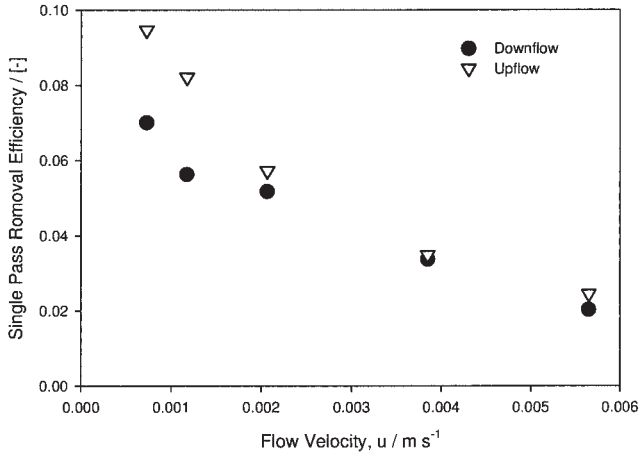

Figure 9. Comparison of flow models for photocatalytic oxidation of PHE in a single-pass run in the OFMR.

Effect of different flow velocities on the single-pass conversion. Geometry: $d_f = 0.001$ m; $\eta = 1/3$. Experimental conditions: $C_{0,\mathrm{PHE}} = 350$ ppb, $I_0 = 3.14 \times 10^4$ mW m^{-2}.

Among the geometric parameters for the OFMR design, fiber diameter affected not only the catalyst coating surface area but also the radiation field by changing the ratio of internal radius to external radius of the annulus and the effective light propagation length. The main bulk solution in the center of the annulus remained untreated as a result of mass transfer limitation as the ratio of fiber radius to channel radius decreased. Reactor length was limited by the effective light propagation length along the titania-coated optical fiber. The conversion efficiency in an OFMR was observed to be higher in the upflow mode than in the downflow mode for water in the reactor.

Further optimization of the laboratory reactor for better utilization of light transmission using optical fibers and higher efficiency of compound degradation are required before any larger pilot-scale applications can be envisaged.

Acknowledgments

This work was supported by a grant from the U.S. EPA through the Gulf Coast Hazardous Substance Research Center, Lamar University, TX. This document has not been subject to Agency review and does not necessarily reflect the views of the U.S. EPA, nor should any endorsement of product names be assumed.

Literature Cited

1. Mills A, Davies RH, Worley D. Water-purification by semiconductor photocatalysis. *Chem Soc Rev.* 1993;22:417-425.
2. Mills A, Le Hunte SJ. An overview of semiconductor photocatalysis. *J Photochem Photobiol A.* 1997;108:1-35.

3. Legrini O, Oliveros E, Braun AM. Photochemical processes for water-treatment. *Chem Rev.* 1993;93:671-698.
4. Hoffmann MR, Martin ST, Choi WY, Bahnemann DW. Environmental applications of semiconductor photocatalysis. *Chem Rev.* 1995;95: 69-96.
5. Herrmann JM. Heterogeneous photocatalysis: Fundamentals and applications to the removal of various types of aqueous pollutants. *Catal Today.* 1999;53:115-129.
6. Alfano OM, Bahnemann D, Cassano AE, Dillert R, Goslich R. Photocatalysis in water environments using artificial and solar light. *Catal Today.* 2000;58:199-230.
7. Ray AK. Design, modelling and experimentation of a new large-scale photocatalytic reactor for water treatment. *Chem Eng Sci.* 1999;54: 3113-3125.
8. Cassano AE, Martin CA, Brandi RJ, Alfano OM. Photoreactor analysis and design—Fundamentals and applications. *Ind Eng Chem Res.* 1995; 34:2155-2201.
9. Brandi RJ, Alfano OM, Cassano AE. Evaluation of radiation absorption in slurry photocatalytic reactors. 1. Assessment of methods in use and new proposal. *Environ Sci Technol.* 2000;34:2623-2630.
10. Puma GL, Khor JN, Brucato A. Modeling of an annular photocatalytic reactor for water purification: Oxidation of pesticides. *Environ Sci Technol.* 2004;38:3737-3745.
11. Raissi AT, Martin ED, Muradov N, Jaganathan S, Painter CR, Kemme MR. Mass transfer considerations in the design of vapor-phase photocatalytic reactors. *J Adv Oxid Technol.* 1998;3:188-198.
12. Lin H, Valsaraj KT. A titania thin film annular photocatalytic reactor for the degradation of polycyclic aromatic hydrocarbons in dilute water streams. *J Hazard Mater.* 2003;99:203-219.
13. Lin H, Valsaraj KT. Development of an optical fiber monolith reactor for photocatalytic wastewater treatment. *J Appl Electrochem.* 2005;35: 699-708.
14. Lin H, Ravikrishna R, Valsaraj KT. Reusable adsorbents for dilute solution separation. 6. Batch and continuous reactors for the adsorption and degradation of 1,2-dichlorobenzene from dilute wastewater streams using titania as a photocatalyst. *Sep Purif Technol.* 2002;28: 87-102.
15. Lin H. *Photocatalysis in a Novel Semiconducting Optical Fiber Monolith Reactor for Wastewater Treatment*. PhD Dissertation. Baton Rouge, LA: Louisiana State University; 2005.
16. Peill N, Hoffmann MR. Mathematical model of a photocatalytic fiber-optic cable reactor for heterogeneous photocatalysis. *Environ Sci Technol.* 1998;32:398-404.
17. Bird RB, Stewart WE, Lightfoot EN. *Transport Phenomena*. 2nd Edition. New York, NY: Wiley; 2002.
18. Gustafson KE, Dickhut RM. Molecular diffusivity of polycyclic aromatic hydrocarbons in aqueous-solution. *J Chem Eng Data.* 1994;39: 281-285.
19. Peill N, Hoffmann MR. Chemical and physical characterization of a TiO_2-coated fiber optic cable reactor. *Environ Sci Technol.* 1996;30: 2806-2812.
20. Marinangelli RE, Ollis DF. Photo-assisted heterogeneous catalysis with optical fibers. Part III: Photoelectrodes. *AIChE J.* 1982;28:945-955.
21. Sauer ML, Ollis DF. Acetone oxidation in a photocatalytic monolith reactor. *J Catal.* 1981;149:81-91.
22. De Lasa H, Serrano B, Salaices M. *Photocatalytic Reaction Engineering*. New York, NY: Springer Science and Business Media; 2005.
23. Kreutzer MT, Kapteijn F, Mouljin JA, Heiszwolf JJ. Multiphase monolith reactors: Chemical reaction engineering of segmented flow in microchannels. *Chem Eng Sci.* 2005;60:5895-5916.

Manuscript received Oct. 19, 2005, and revision received Feb. 7, 2006.